A&A 589, A5 (2016)
DOI: 10.1051/0004-6361/201527727

Astronomy & Astrophysics

A search for hydrogenated fullerenes in fullerene-containing planetary nebulae

J. J. Díaz-Luis[1,2], D. A. García-Hernández[1,2], A. Manchado[1,2,3], and F. Cataldo[4,5]

[1] Instituto de Astrofísica de Canarias, C/ Via Láctea s/n, 38205 La Laguna, Spain
e-mail: [jdiaz;agarcia]@iac.es
[2] Departamento de Astrofísica, Universidad de La Laguna (ULL), 38206 La Laguna, Spain
[3] Consejo Superior de Investigaciones Científicas, Madrid, Spain
[4] INAF–Osservatorio Astrofisico di Catania, via S. Sofia 78, 95123 Catania, Italy
[5] Actinium Chemical Research srl, via Casilina 1626/A, 00133 Rome, Italy

Received 11 November 2015 / Accepted 19 February 2016

ABSTRACT

Detections of C_{60} and C_{70} fullerenes in planetary nebulae (PNe) of the Magellanic Clouds and of our own Galaxy have raised the idea that other forms of carbon, such as hydrogenated fullerenes (fulleranes like $C_{60}H_{36}$ and $C_{60}H_{18}$), buckyonions, and carbon nanotubes, may be widespread in the Universe. Here we present VLT/ISAAC spectra ($R \sim 600$) in the 2.9−4.1 μm spectral region for the Galactic PNe Tc 1 and M 1−20, which have been used to search for fullerene-based molecules in their fullerene-rich circumstellar environments. We report the non-detection of the most intense infrared bands of several fulleranes around ∼3.4−3.6 μm in both PNe. We conclude that if fulleranes are present in the fullerene-containing circumstellar environments of these PNe, then they seem to be much less abundant than C_{60} and C_{70}. Our non-detections, together with the (tentative) fulleranes detection in the proto-PN IRAS 01005+7910, suggest that fulleranes may be formed in the short transition phase between AGB stars and PNe, but they are quickly destroyed by the UV radiation field from the central star.

Key words. astrochemistry – line: identification – circumstellar matter – molecular processes – stars: AGB and post-AGB – planetary nebulae: general

1. Introduction

Fullerenes, highly resistant and stable tridimensional molecules that are formed exclusively by carbon atoms, have attracted much attention since their discovery in a laboratory by Kroto et al. (1985); C_{60} and C_{70} are the most abundant fullerenes. Fullerenes and fullerene-based molecules, such as hydrogenated fullerenes and buckyonions, may explain some astrophysical phenomena, like the intense UV absorption band at 217 nm (e.g., Cataldo & Iglesias-Groth 2009) or the so-called diffuse interstellar bands (DIBs; see e.g., Cox 2011; Iglesias-Groth 2007; García-Hernández & Díaz-Luis 2013; Díaz-Luis et al. 2015). Owing to the remarkable stability of fullerenes against intense radiation and ionization, these molecules are good candidates for being widespread in insterstellar/circumstellar media. Their presence in astrophysical environments have recently been confirmed by the *Spitzer* Space Telescope via the detection of the mid-infrared C_{60} and C_{70} fullerene features in the spectrum of the young planetary nebula (PN) Tc 1 (Cami et al. 2010).

The detection of fullerenes in Tc 1 was interpreted as being due to the H-poor conditions in the nebular core (since there is no polycyclic aromatic hydrocarbons (PAHs) emission; Cami et al. 2010), in agreement with some laboratory studies (e.g., Kroto et al. 1985), which show that fullerenes are efficiently produced in the absence of hydrogen. However, it has been demonstrated that fullerenes are efficiently formed only in H-rich circumstellar environments (García-Hernández et al. 2010, 2011b), challenging our previous understanding of the formation of fullerenes in space. In particular, the simultaneous detection of C_{60} fullerenes and PAHs in several PNe with normal hydrogen abundances has been reported (García-Hernández et al. 2010, 2011a, 2012; Otsuka et al. 2014). García-Hernández et al. (2010) propose that both fullerenes and PAHs in H-rich circumstellar ejecta may form from the photochemical processing of hydrogenated amorphous carbon (HAC) in agreement with the experimental results of Scott et al. (1997)[1]. In addition, the first evidence of the possible detection of planar C_{24} (a piece of graphene) in some of these fullerene-containing sources has been reported (García-Hernández et al. 2011a), which raises the idea that other forms of carbon such as hydrogenated fullerenes (fulleranes such as $C_{60}H_{36}$ and $C_{60}H_{18}$), buckyonions, or carbon nanotubes, may be widespread in the Universe.

Duley & Williams (2011) predict the production of fullerenes via thermal heating of HAC and this process may explain the detection of fullerenes in H-rich circumstellar environments (e.g., García-Hernández et al. 2010). Interestingly, they also predict the formation of hydrogenated fullerenes (fulleranes). On the other hand, Iglesias-Groth et al. (2012) found that the 3.44 and 3.55 μm bands of several fulleranes display molar extinction coefficients that are similar to those of the 17.4 and 18.8 μm bands of the isolated C_{60} molecule (Iglesias-Groth et al. 2011). Thus, it could be reasonable to find fulleranes

[1] Duley & Hu (2012) suggest that the IR features at ∼7.0, 8.5, 17.4, and 18.8 μm detected in objects with PAH-like-dominated IR spectra, such as those of R Coronae Borealis stars (García-Hernández et al. 2011b), reflection nebulae (Sellgren et al. 2010), or proto-PNe (Zhang & Kwok 2011) should be attributed to proto-fullerenes (or fullerene precursors) instead of C_{60}.

Table 1. Observational parameters of fullerene PNe and their comparison stars.

Object	l	b	$E(B-V)$	V_r	Ref.[a]	Telluric/flux star	l	b	SpT	V_r	Ref.[a]
Tc 1	345.2375	−08.8350	0.23	−94.0	1, 2	HR 7446	31.7709	−13.2866	B0.5III	−19.4	4, 5
M 1−20	6.187	8.362	0.80	75.0	2, 3	HIP 92519	351.7764	−18.6123	G0V	70.9	4, 6

References. [(a)] (1) Williams et al. (2008); (2) Beaulieu et al. (1999); (3) Wang & Liu (2007); (4) De Bruijne & Eilers (2012); (5) Wegner (2003); (6) Soubiran et al. (2013).

with line intensities similar to the ones already measured with *Spitzer* at 17.4 and 18.8 μm in fullerene-containing PNe. Indeed, Zhang & Kwok (2013) have tentatively detected fulleranes in the Infrared Space Observatory (ISO) spectrum of the proto-PN IRAS 01005+7910, where three emission peaks at ∼3.48, 3.51, and 3.58 μm in the C-H stretching region seem to be present.

More recently, several fullerene-based molecules, like fullerene/PAH adducts, have been synthesized and characterized in the laboratory (e.g., García-Hernández et al. 2013; Cataldo et al. 2014, 2015). Remarkably, fullerene/PAH adducts such as C_{60}/anthracene display mid-IR ($\lambda > 5$ μm) spectral features that are strikingly coincident with those from C_{60} and C_{70} (García-Hernández et al. 2013) and it is still no clear if these species could contribute to the observed C_{60} (and C_{70}) features in fullerene-rich environments. Laboratory spectra of C_{60}/anthracene adducts display the typical aromatic bands around 3.3 μm, as well as aliphatic C−H bands at ∼3.39, 3.43, and 3.52 μm, which are not present in the C_{60} and C_{70} spectra. In principle, this could be used to elucidate the possible carrier (e.g., C_{60} versus C_{60}/PAH adducts) of the mid-IR features seen in fullerene PNe. However, the C−H stretching bands are intrinsically weaker than the other emission features at longer wavelengths and the presence of these C−H stretching bands (typical for CH_2 and CH_3 groups of several carbonaceous materials) is not yet completely understood (García-Hernández et al. 2013), which complicates the search of these fullerene-related species in space.

In this paper, we present VLT/ISAAC spectroscopy (the 2.9−4.1 μm spectral region) of two PNe with fullerenes (Tc 1 and M 1−20). An overview of the spectroscopic observations is presented in Sect. 2; together with a summary of the nebular emission lines observed. Section 3 presents a brief discussion of the detection of the 3.3 μm unidentified infrared emission (UIE) feature in our VLT/ISAAC spectrum of M 1−20 and its possible carriers. Section 4 discusses the non-detection of infrared emission bands (e.g., from fulleranes) in our spectra. The conclusions of our work are given in Sect. 5.

2. Mid-infrared VLT/ISAAC spectroscopy of PNe with fullerenes

We acquired 3-4 μm infrared (IR) spectra of the fullerene PNe Tc 1 ($W1[3.35\,\mu m]_{WISE} = 8.19$, $E(B-V) = 0.23$; Cutri et al. 2012; Williams et al. 2008) and M 1−20 ($W1[3.35\,\mu m]_{WISE} = 9.65$, $E(B-V) = 0.80$; Cutri et al. 2012; Wang & Liu 2007) with a signal-to-noise ratio (at the continuum in the final IR spectra) of ∼26 and 11, respectively. Tc 1 displays a fullerene-dominated spectrum with no clear signs of PAHs, while M 1−20 also shows weak PAH-like features (see, e.g., García-Hernández et al. 2010). Table 1 lists some observational parameters such as Galactic coordinates, color excess and radial velocity for the two fullerene PNe in our sample and the corresponding telluric/flux stars for each PN.

The observations of Tc 1, M 1−20, and their corresponding telluric/flux standards were carried out at the ESO VLT (Paranal, Chile) with ISAAC in service mode between 14−23 July 2013. We used the LWS-LR/3550 nm set-up with the 0.6″ slit oriented at a position angle of 0°. This configuration covers the spectral range 2.9−4.1 μm and gives a resolving power of ∼600, which is required to cleanly separate the 3−4 μm features of several fullerene-based molecules as seen in the laboratory. During the observations, the seeing was about 0.5−0.6 and 1.5−1.7 arcsec for Tc 1 and M 1−20 (and their corresponding standards), respectively.

The spectra were obtained combining the chopping technique (moving the secondary mirror of the telescope once every few seconds) with telescope nodding. We used a total integration time of 38 min for each observing block (OB). For Tc 1, we obtained three OBs of 26 individual exposures each, giving a total exposure time of ∼1.9 h, and for M 1−20, one OB of ∼38 min. Raw spectra were processed by the ISAAC data reduction pipeline[2] in conjunction with the data browsing tool GASGANO[3]. In short, i) flat-fields are combined to produce a master flat-field; ii) the wavelength calibration and ISAAC slit curvature distortion is computed using OH sky lines; and iii) the removal of the high degree of curvature of ISAAC spectra is performed by calculating the spectra curvature using a star moving across the slit. Thus, science frames were reduced using the products of the pipeline calibration recipes. The produced 2D image for each PN is then used to extract the one-dimensional spectrum across the defined apertures with IRAF[4]. We note that the continuum emission is not extended in both PNe but, to cover the nebular hydrogen lines in the 2D images, we needed to define an aperture of 78 and 10 pixels for Tc 1 and M 1−20, which translate (scale of 0.15 arcsec/pixel) into nebular extensions of ∼11.5 and ∼1.5 arcsec, respectively. Finally, the extracted spectra were combined to produce a final, reduced science spectrum. This process was also done for the telluric stars, which are also used for flux calibration (see below).

We used the telluric stars to determine the sensitivity and extinction functions to flux calibrate our science spectra with standard tasks in IRAF. We assumed that the two stars behave approximately like black bodies. There are two parameters needed to scale the black body to the observation: the magnitude of the star in the same band as the observation (L-band at 3.4 μm) and the effective temperature. The estimated flux errors are approximately 30−40%. Finally, telluric correction was made using the telluric star for each PN.

[2] https://www.eso.org/sci/software/pipelines/isaac/isaac-pipe-recipes.html

[3] https://www.eso.org/sci/software/gasgano.html

[4] Image reduction and analysis facility (IRAF) software is distributed by the National Optical Astronomy Observatories, which are operated by the Association of Universities for Research in Astronomy, Inc., under cooperative agreement with the National Science Foundation.

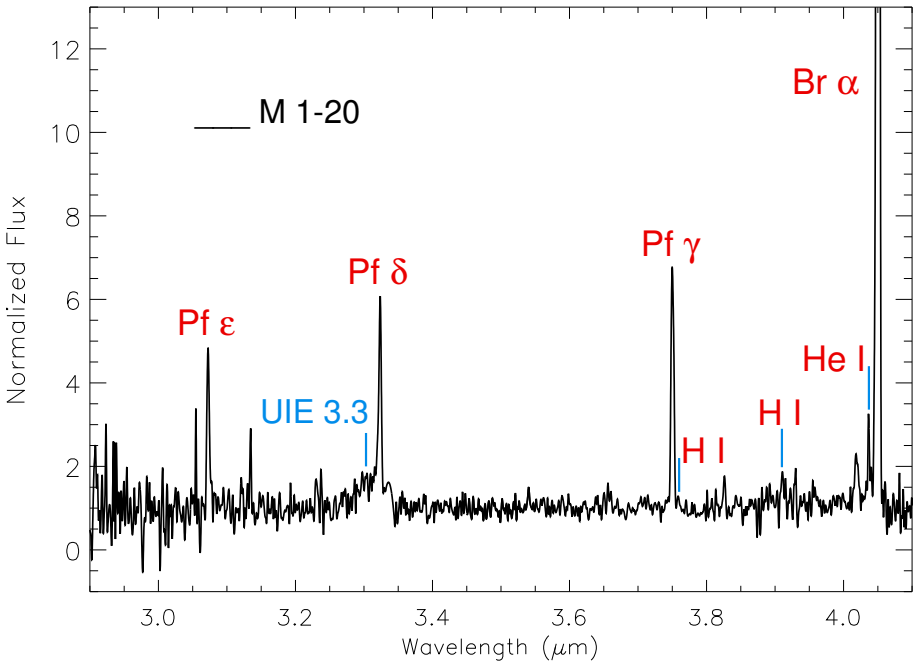

Fig. 1. VLT/ISAAC spectrum of PN M 1−20. The atomic H lines of the Pfund series (Pf_ϵ, Pf_δ and Pf_γ), H I (6−17), H I (6−15), and Br_α, as well as the UIE feature at 3.3 μm and the line of He I (4−5), are indicated.

Table 2. Nebular emission lines identified in the 2.9-4.1 μm spectra of M 1−20 and Tc 1.

Element	M 1−20 λ_c (μm)	*FWHM* (10^{-4} μm)	FLUX[a] (10^{-15}erg cm^{-2} s^{-1})	Tc 1 λ_c (μm)	*FWHM* ($10^{-4}\mu$m)	FLUX[a] (10^{-15}erg cm^{-2} s^{-1})
H I (Pf_ϵ)	3.07	43.68	4.20			
UIE	3.31	536.10	17.20			
H I (Pf_δ)	3.32	41.05	6.49	3.30	37.88	0.28
H I (Pf_γ)	3.75	45.96	5.74	3.74	47.32	0.43
H I (6−17)	3.76	40.95	0.33	3.75	42.43	0.03
H I (6−15)	3.91	40.45	0.54	3.90	37.77	0.04
He I (4−5)	4.04	25.01	0.86	4.04	43.17	0.11
H I (Br_α)	4.05	47.59	46.70	4.05	48.48	3.49

Notes. [(a)] Estimated flux errors are of the order of ∼30%–40%.

2.1. Nebular emission lines

In this section, we give an overview of the nebular emission lines that were observed in the 2.9 to 4.1 μm region. This spectral range is dominated by nebular emission lines of hydrogen.

Our list of features in Tc 1 and M 1−20 is shown in Table 2, where we give the measured central wavelength (λ_c), the full width at half maximum (FWHM), the equivalent width (EQW), and the integrated flux[5].

The M 1−20 spectrum includes the atomic hydrogen lines Pf_ϵ at 3.07 μm, a blend of the UIE feature at 3.31 with Pf_δ at 3.32 μm, Pf_γ at 3.75 μm, and Br_α at 4.05 μm. It also includes the tentatively identified H I (6−17), H I (6−15), and He I (4−5) lines at 3.76, 3.91, and 4.04 μm, respectively. In Fig. 1, we display the M 1−20 spectrum in the 2.9-4.1 μm range.

The Tc 1 spectrum includes the atomic hydrogen lines Pf_δ, Pf_γ, the tentatively identified H I (6−17) and H I (6−15) lines, and Br_α. It also includes the tentative He I (4−5) line at 4.04 μm. In Fig. 2, we display the Tc 1 2.9−4.1 μm spectrum.

[5] The feature parameters were measured with IRAF by assuming a Gaussian profile.

3. The 3.3 μm UIE feature

We clearly detect the 3.3 μm UIE feature in M 1−20, while this feature is completely lacking in Tc 1. This is consistent with the *Spitzer* spectra; M 1−20 displays UIE features (PAH-like) at 6.2, 7.7, 8.6, and 11.3 μm, but these are absent in Tc 1 (e.g., García-Hernández et al. 2010). The detected UIE feature in the M 1−20 spectrum was fitted with a Gaussian to determine the feature's FWHM and central wavelength. Owing to the emission line of H I (Pf_δ) at 3.32 μm, it was necessary to deblend both features. The average central wavelength of the UIE feature was 3.31 μm, with a FWHM of 0.05 μm. This is consistent with the values measured by Tokunaga et al. (1991) and Smith & McLean (2008; average values of $\lambda_c \sim 3.29$ μm and *FWHM* ~ 0.04 μm) in extended objects such as PNe, (proto-) PNe, and H II regions. In Fig. 1, we can see the 3.3 μm UIE feature in the M 1−20 spectrum blended with the Pf_δ hydrogen emission line at 3.32 μm.

3.1. Possible carriers of the 3.3 μm UIE feature

The 3.3 μm feature belongs to the group of UIE features or aromatic infrared bands (AIBs) at 3.3, 6.2, 7.7, 8.6, 11.3, and 12.7 μm. These bands may be accompanied by aliphatic bands at 3.4, 6.9, and 7.3 μm, and unassigned features at 15.8, 16.4, 17.4,

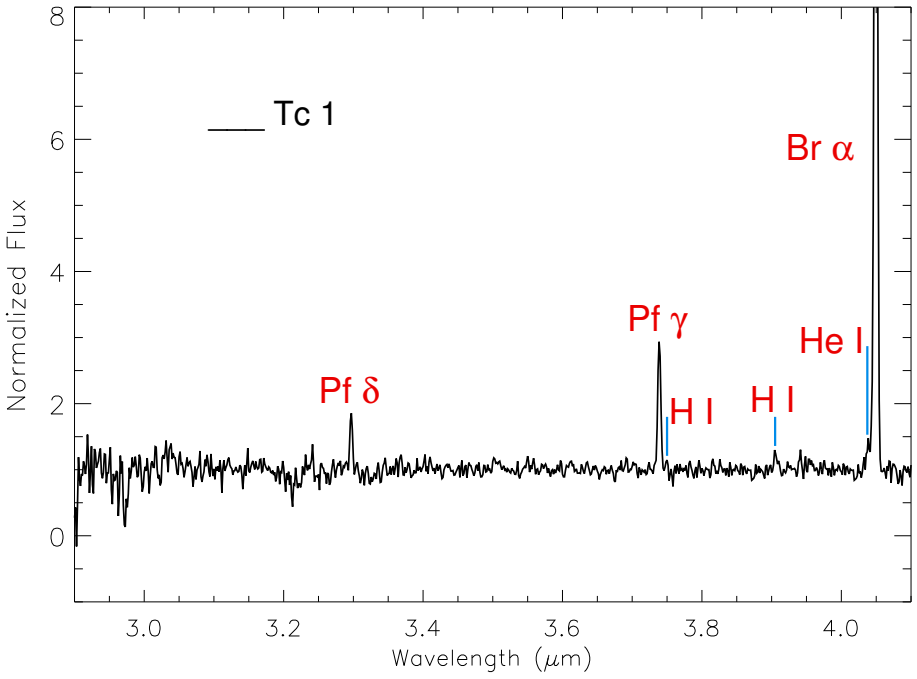

Fig. 2. VLT/ISAAC spectrum of Tc 1. The atomic H lines of the Pfund series (Pf_{δ} and Pf_{γ}), H I (6−17), H I (6−15), and Br_{α}, as well as the line of He I (4−5), are indicated.

17.8, and 18.9 μm (Jourdain de Muizon et al. 1990; Kwok et al. 1999; Chiar et al. 2000; Sturm et al. 2000; Sellgren et al. 2007)[6], and the broad emission features at ∼6−9, 9−13, 15−20, and 25−35 μm, which are believed to be produced by a carbonaceous mixture of aromatic and aliphatic structures (e.g., HAC, coal, petroleum fractions, etc.), and/or their decomposition products (García-Hernández et al. 2010, 2012; Kwok & Zhang 2011). The 11.3 μm UIE feature is found to be correlated with the 3.3 μm feature (Russell et al. 1977), which suggests a common origin for the two features. This correlation holds for fullerene PNe; we detect the weak UIE feature at 3.3 μm in our VLT/ISAAC spectrum and the M 1−20 *Spitzer* spectrum shows a very strong aromatic-like infrared band at 11.3 μm (García-Hernández et al. 2012), while Tc 1 displays a very weak emission at 11.3 μm and it does not show the feature at 3.3 μm.

A wide variety of molecules have been proposed as possible carriers of these 3.3 and 11.3 μm UIE bands. Currently, the most accepted idea is that they originate from the C-H vibration modes of aromatic compounds or PAHs (e.g., Duley & Williams 1981; Leger & Puget 1984; Allamandola et al. 1985). However, Sadjadi et al. (2015) calculated the out-of-plane (OOP) bending mode frequencies of 60 neutral PAH molecules and found that it is difficult to fit the 11.3 μm UIE feature. This feature cannot be fitted by superpositions of pure PAH molecules, and O- (and or Mg-) containing species are needed to achieve a good fit, suggesting that the PAHdb model (Bauschlicher et al. 2010; Boersma et al. 2014) has problems explaining the UIE phenomenon (see Sadjadi et al. 2015 for more details). Maltseva et al. (2015) also found difficulties for predicting high-resolution experimental absorption spectra of PAHs in the 3 μm region with harmonic density functional theory (DFT) calculations. However, their anharmonic DFT calculations work well for small PAHs in this spectral region, opening the way to predict the spectrum of larger PAHs (and other hydrocarbons). Finally, Gadallah et al. (2013) also found that the 3.3 μm and 6.2 μm AIBs are also clearly observed in the spectrum of heated HAC dust.

On the other hand, Duley & Williams (2011) suggest a model in which the astronomical emission at 3.3 μm can be explained by the heating of HAC dust via the release of stored chemical energy. This energy could be sufficient to heat dust grains (with sizes of ∼50−1000 Å) to temperatures at which they can emit at 3.3 μm. This alternative to the PAH hypothesis involves a solid material with a mix of aliphatic and aromatic structures (i.e., HACs), which may explain the broad emission features at ∼6−9, 9−13, 15−20, and 25−35 μm detected in PNe with fullerenes (García-Hernández et al. 2010, 2012) and most C-rich proto-PNe. Moreover, laboratory experiments show that the products of destruction of HAC grains are PAHs and fullerenes (Scott et al. 1997), something that could explain the detection of both types of molecules in some fullerene PNe (García-Hernández et al. 2010). Unfortunately, our VLT/ISAAC observations do not add much information about the real carrier (e.g., PAHs vs. HACs) of the 3.3 μm emission. The non-detection of 3.3 μm emission in Tc 1 may suggest a different spatial distribution of the 3.3 μm carrier and the C_{60} (and C_{70}) fullerenes. Bernard-Salas et al. (2012) already found that the *Spitzer* C_{60} 8.5 μm and weak 11.2 μm emission (which likely share the same carrier with the 3.3 μm emission, see above) are extended, but they peak at opposite directions from the Tc 1 central star[7]. The *Spitzer* observations (slit of ∼4″ × 57″ at a PA of 0 deg) show extended emission up to ∼22″ (Bernard-Salas et al. 2012), while our VLT/ISAAC spectra, taken with a smaller slit of 0.6 arcsec, show no extended emission at 3.3 μm. Thus, it could be possible that we are missing the weak 3.3 μm emission in the ISAAC observations (e.g., a small column density throughout the circumstellar envelope). In the case of the more compact (apparent size of ∼2 arcsec) PN M 1−20, we have no spatial information from the *Spitzer* spectra (which covered the entire nebula) and the 3.3 μm emission in the VLT/ISAAC spectra is not extended.

In short, it is still not clear if the emission bands at 3.3 and 11.3 μm seen in PNe with fullerenes are only due to pure

[6] It is now known that the 17.4 and 18.9 μm features are due to fullerenes.

[7] Sellgren et al. (2010) reported a similar separation in the spatial distribution of the fullerene and PAH emission seen in the fullerene-containing reflection nebula NGC 7023.

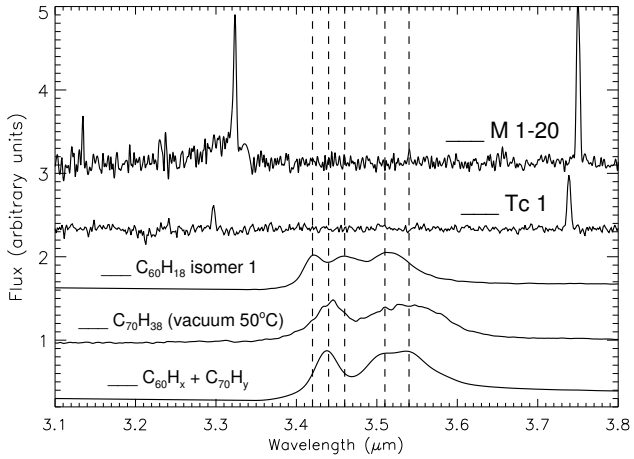

Fig. 3. VLT/ISAAC spectra of M 1−20 and Tc 1, in comparison with the laboratory spectra of the fulleranes $C_{60}H_{18}$, $C_{70}H_{38}$, and $C_{60}H_x$+$C_{70}H_y$ in the 3.1−3.8 μm range. Note that the $C_{60}H_{18}$ fullerane bands at 3.42, 3.46, and 3.51 μm and the $C_{70}H_{38}$ fullerane bands at 3.44 and 3.54 μm are marked with dashed lines. The $C_{60}H_x$+$C_{70}H_y$ fullerane bands are those at 3.44, 3.51, and 3.54 μm.

aromatic compounds or to mixed aromatic/aliphatic structures, such as those of HAC-like dust.

4. Non-detection of the fullerane features

The IR laboratory spectra ($R \sim 500$) of several fulleranes, such as $C_{60}H_{18}$, $C_{60}H_{36}$, or $C_{70}H_{38}$ (Iglesias-Groth et al. 2012), show that the strongest features in the mid-IR (2−20 μm) are those at ~3.44, 3.51, and 3.54 μm[8] (see Fig. 3), being the best *IR* bands for searching these molecules in the circumstellar environments of fullerene-rich PNe. Thus, at the resolution ($R \sim 600$) of the VLT/ISAAC observations, it is possible to easily resolve these bands, as well as to distinguish them from the 3.3 μm emission (Iglesias-Groth et al. 2012). However, none of these three emission features is detected in our VLT/ISAAC spectra of Tc 1 and M 1−20. Figure 3 shows the non-detection of the fullerane features between 3.4 and 3.6 μm in our VLT/ISAAC spectra of Tc 1 and M 1−20. The laboratory spectra of the fulleranes $C_{60}H_{18}$, $C_{70}H_{38}$, and $C_{60}H_x$+$C_{70}H_y$ (see below) are also displayed and their corresponding 3.4−3.6 μm features are indicated.

We could estimate approximate upper limits to the fluxes of the hydrogenated fullerene features (see Table 3). To obtain 2σ upper limits to the expected emission line fluxes of the fullerane features at ~3.5 μm, we measure the rms in our flux-calibrated VLT/ISAAC spectra; rms values of $\sim 4.28 \times 10^{-19}$ erg cm^{-2} s^{-1} Å^{-1} and $\sim 6.65 \times 10^{-18}$ erg cm^{-2} s^{-1} Å^{-1} for Tc 1 and M 1−20 are obtained, respectively. Then we multiply these values by the widths (FWHMs in the range 0.02−0.10 μm) of the fullerane bands, as measured in the infrared laboratory spectra[9]. We used the laboratory spectra of two $C_{60}H_{18}$ isomers (that were obtained using hydrogen iodide and direct hydrogenation with metal hydrides), two $C_{60}H_{36}$ spectra at +48 °C and +250 °C, two $C_{70}H_{38}$ spectra at +50 °C and +160 °C, and the fullerane mixture 77% of $C_{60}H_x$ and 22% $C_{70}H_y$ with $x \approx y \geq 30$ at +45 °C (see Iglesias-Groth et al. 2012 for more details). Finally, we divided these fluxes by the area (~0.6″ arcsec^2 for both PNe) of the emission in the 3−4 μm range covered by our ISAAC observations.

On the other hand, by using the molar absorptivity values for the fullerenes and fulleranes that have been reported by Iglesias-Groth et al. (2011, 2012), we can estimate the predicted fluxes for the fullerane features in Tc 1 and M 1−20[10] (see Table 3). By taking the molar absorptivity ratio (e.g., $\epsilon_{C_{60}}/\epsilon_{\text{fulleranes}}$) of the fullerene and fullerane bands and the observed fluxes of the C_{60} and C_{70} infrared bands that were less contaminated by other species (García-Hernández et al. 2012), we estimate the expected flux of the fullerane features at ~3.5 μm. We note that this is only an approximation and a complete model for the excitation/emission of both species is needed. The *Spitzer* integrated fluxes of the infrared bands at 8.5 and 17.4 μm (C_{60}), and 14.9 μm (C_{70}) are taken from García-Hernández et al. (2012) and converted to flux/arcsec^2 by considering the area covered by the fullerenes emission in the *Spitzer* spectra of Tc 1 (~80 arcsec^2 at 8.5 μm and ~53 arcsec^2 at 14.9 and 17.4 μm) and M 1−20 (~4 arcsec^2 at 8.5, 14.9, and 17.4 μm).

Table 3 shows some examples of the estimated 2σ upper limits and the predicted fluxes for the fullerane bands. For example, the molar absorptivity ratio of the $C_{60}H_{36}$ band at 3.44 μm and the C_{60} infrared band at 8.5 μm is $\epsilon_{8.5}/\epsilon_{3.44} \sim 0.34$. Thus, the expected flux of the $C_{60}H_{36}$ band at 3.44 μm in Tc 1 and M 1−20 would be $\sim 22.13 \times 10^{-14}$ erg cm^{-2} s^{-1}/arcsec^2 and $\sim 5.58 \times 10^{-13}$ erg cm^{-2} s^{-1}/arcsec^2, respectively (see Table 3). Similar values are obtained for the fullerane $C_{60}H_{36}$ band at 3.54 μm, with expected fluxes of $\sim 16.23 \times 10^{-14}$ erg cm^{-2} s^{-1}/arcsec^2, and $\sim 4.11 \times 10^{-13}$ erg cm^{-2} s^{-1}/arcsec^2 in Tc 1 and M 1−20, respectively. In summary, the expected fluxes for all fullerane bands of $C_{60}H_{18}$, $C_{60}H_{36}$, $C_{70}H_{38}$, and the mixture $C_{60}H_x$+$C_{70}H_y$ (by using the observed *Spitzer* fluxes of the C_{60} 8.5 and 17.4 μm and C_{70} 14.9 μm bands) are in the range of $\sim 1.7-30 \times 10^{-14}$ and $\sim 1.4-5.6 \times 10^{-13}$ erg cm^{-2} s^{-1}/arcsec^2 in Tc 1 and M 1−20, respectively (see Table 3 for some representative examples).

By comparing the values of the predicted fluxes with our 2σ upper limits (Table 3), we find that the expected fluxes are a factor of ~20−1000 and ~10−100 higher than the 2σ upper limits for Tc 1 and M 1−20, respectively. From these estimations, we thus conclude that if fulleranes are present in Tc 1 and M 1−20, then they seem to be much less abundant than C_{60} and C_{70}.

As we mentioned above, thermal heating via chemical reactions internal to HAC dust may explain the detection of fullerenes in the H-rich circumstellar environments of PNe, which could potentially form fulleranes (Duley & Williams 2011). In addition, Duley & Hu (2012) reported that laboratory spectra of HAC nano-particles that contain fullerene precursors (or proto-fullerenes; PFs), but not C_{60}, display the same set of mid-IR features as the isolated C_{60} molecule. They suggest an evolutionary sequence for the conversion of HAC to fullerenes, in which initial HAC de-hydrogenation is followed by PF formation and subsequent conversion of PFs to closed cage structures such as C_{60}. Under the Duley & Hu (2012) scenario, Tc 1 would represent the last stage in the HAC dehydrogenation process (i.e., only fullerenes are present), while the proto-PN IRAS 01005+7910 would represent an intermediate stage where the PFs are being converted to fullerenes. Of note, fulleranes may also be by-products of this conversion from HAC to fullerenes (Duley & Hu 2012).

[8] Fulleranes do not emit at 3.3 μm because they lack sp^2-bonded CH groups (see Fig. 3).

[9] Note that Zhang & Kwok (2013) measured similar FWHMs (in the range ~0.02−0.04 μm) for the posssible fullerane bands seen in the ISO spectrum of IRAS 01005+7910.

[10] The molar absorptivities of fullerenes and fulleranes are determined with the same standard procedure (Iglesias-Groth et al. 2011, 2012) and we used them to estimate the predicted fluxes.

Table 3. Summary table showing examples of the expected fluxes for the fullerane features.

Fullerane	λ_c (μm)	*FWHM* ($10^{-2}\mu$m)	FLUX[a] (Tc 1) (10^{-16} erg cm^{-2} s^{-1}/$''^2$)	Predicted fluxes (Tc 1) (10^{-14}erg cm^{-2} s^{-1}/$''^2$)	FLUX[a] (M 1−20) (10^{-15} erg cm^{-2} s^{-1}/$''^2$)	Predicted fluxes (M 1−20) (10^{-13}erg cm^{-2} s^{-1}/$''^2$)
$C_{60}H_{18}$ (isomer 1)	3.42	2.1	≤3.00	9.43[b]	≤4.65	2.39[b]
	3.46	3.6	≤5.13	10.20[b]	≤7.98	2.58[b]
	3.51	5.1	≤7.28	13.25[b]	≤11.30	3.36[b]
$C_{60}H_{18}$ (isomer 2)	3.42	2.2	≤3.13	12.74[c]	≤4.87	1.42[c]
	3.45	3.4	≤4.85	13.92[c]	≤7.53	1.56[c]
	3.51	5.5	≤7.85	18.21[c]	≤12.18	2.06[c]
$C_{60}H_{36}$ (+48°C)	3.44	2.3	≤3.33	22.13[b]	≤5.18	5.58[b]
	3.54	7.7	≤11.02	16.23[b]	≤17.10	4.11[b]
$C_{60}H_{36}$ (+250°C)	3.44	2.2	≤3.10	30.11[c]	≤4.80	3.39[c]
	3.53	10.1	≤14.38	22.08[c]	≤22.33	2.47[c]
$C_{70}H_{38}$ (+50°C)	3.44	2.5	≤3.62	18.13[b]	≤5.63	4.61[b]
	3.54	7.0	≤10.05	16.75[b]	≤15.62	4.22[b]
$C_{70}H_{38}$ (+160°C)	3.44	2.5	≤3.55	1.81[d]	≤5.52	2.72[c]
	3.54	6.3	≤8.97	1.68[d]	≤13.93	2.56[c]
$C_{60}H_x$+$C_{70}H_y$ (+45°C)	3.44	2.2	≤3.13	20.13[b]	≤4.87	5.08[b]
	3.51	2.8	≤4.00		≤6.20	
	3.54	2.5	≤3.57	18.71[b]	≤5.53	4.75[b]

Notes. Quoted values are the measured central wavelengths of the fullerane features, the full widths at half maximum (FWHM), the 2σ upper detection limits to the expected emission line fluxes in Tc 1 and M 1−20, and the predicted fluxes for the fullerane bands. [(a)] Estimated flux errors are ∼30%−40%. [(b)] Flux prediction obtained by taking the observed flux of the C_{60} feature at ∼8.5 μm. [(c)] Flux prediction obtained by taking the observed flux of the C_{60} feature at ∼17.4 μm. [(d)] Flux prediction obtained by taking the observed flux of the C_{70} feature at ∼14.9 μm.

Interestingly, Zhang & Kwok (2013) have (tentatively) detected fulleranes in the proto-PN IRAS 01005+7910; three strong C-H stretching bands at 3.48, 3.51, and 3.58 μm are apparently present in its ISO spectrum with fluxes that are comparable to the one of the 3.3 μm feature. By assuming that all features have the same oscillator strength, they conclude that the calculated relative strengths indicate that the m value (degree of hydrogenation of the fulleranes $C_{60}H_m$) may lie within the range from 25−40, which is consistent with the production of $C_{60}H_{36}$ (the dominant product of the hydrogenation reaction of C_{60}; e.g., Cataldo & Iglesias-Groth 2009)[11]. In addition, the observed fluxes of the C_{60} and fullerane bands suggest that about 50 percent of fullerenes have been hydrogenated. Curiously, IRAS 01005+7910 displays exceptionally strong C_{60}^+ DIBs (Iglesias-Groth & Esposito 2013).

Our non-detection of fulleranes in more evolved PNe (such as Tc 1 and M 1-20 with $T_{\rm eff} > 30\,000$ K) together with their possible detection in less evolved sources (like IRAS 01005+7910 with $T_{\rm eff} \sim 21\,500$ K) thus suggest that fulleranes may be formed in the short transition phase between asymptotic giant branch (AGB) stars and PNe but they are quickly destroyed; e.g., they are photochemically processed by the rapidly changing UV radiation from the central star. The rapid increase of the UV radiation towards the PN stage will easily break the C−H bonds of the previously formed fullerane molecules, forming fulleranes at lower hydrogenation degree or reforming – more resistant – C_{60} and C_{70} fullerenes and molecular hydrogen (Cataldo & Iglesias-Groth 2009). However, it is still not clear what the origin of fulleranes is. Fulleranes could be formed via the Duley & Hu (2012) HAC de-hydrogenation process, mentioned above, in which fulleranes may be by-products from the conversion from PFs to C_{60}, or they could be formed by the reaction of pre-existing fullerenes (e.g., formed by the photochemical processing of HACs; Scott et al. 1997) with atomic hydrogen. During the short (∼10^2–10^4 yr) transition phase, AGB-PN, H_2[12] may be photodissociated into atomic H owing to the gradual increase of the UV radiation field with the evolution of the central star and/or by shocks (H_2 dissociated through collisions) as a result of the fast post-AGB stellar winds. By reacting with atomic hydrogen, fullerenes form fulleranes at various degrees of hydrogenation. Thus, the post-AGB phase could make the reaction between fullerenes and atomic H more favorable (Cataldo & Iglesias-Groth 2009) and it seems to provide the right conditions for the formation and detection of fulleranes.

5. Conclusions

We have presented VLT/ISAAC 2.9−4.1 μm spectroscopy of two fullerene PNe in our Galaxy. The spectrum of Tc 1 shows a continuum with no signs of UIE features and only H (and He) nebular lines. This indicates that the IR bands seen in the Tc 1 *Spitzer* spectrum are very likely due to C_{60} and C_{70} alone, and not other kinds of molecules, such as fulleranes or fullerene/PAH adducts. The M 1−20 VLT/ISAAC spectrum shows H and He nebular lines in conjunction with the UIE feature at 3.3 μm.

The VLT/ISAAC and *Spitzer* spectra of these fullerene PNe confirm a correlation between the 3.3 and 11.3 μm UIE features, as previously reported in the literature, which suggests a common carrier for the two features. Unfortunately, the VLT/ISAAC observations, presented here, cannot reveal the nature of the real carrier (e.g., PAHs vs. HACs) of the 3.3 μm emission.

Interestingly, we have reported the non-detection of the strongest bands of hydrogenated fullerenes (fulleranes such as $C_{60}H_{18}$, $C_{60}H_{36}$, $C_{70}H_{38}$, and a fullerane mixture) at ∼3.44, 3.51 and 3.54 μm in the 3−4 μm spectra of the fullerene-containing PNe Tc 1 and M 1−20. From a comparison of the predicted fluxes of the fullerane bands with our 2σ upper limits, we conclude that, if fulleranes are present in both objects, then they seem to be much less abundant than isolated fullerene molecules.

[11] Zhang & Kwok (2013) suggest that $C_{60}H_{18}$ might be also present.

[12] The HAC chemical energy model of Duley & Williams (2011) also predicts the release of warm H_2 molecules trapped inside the HAC solid.

Our non-detection of fulleranes in two fullerene PNe, together with their possible detection (if real) in the fullerene proto-PN IRAS 01005+7910, suggests that these fullerene-related species may be formed in the short transition phase AGB−PN, but they are rapidly destroyed; e.g., by the quick increase of UV radiation from the central star towards the PN stage. The transition between AGB stars and PNe seems to be the best evolutionary stellar phase for finding fulleranes in space and 3−4 μm spectroscopy in a larger sample of C-rich proto-PNe is encouraged.

Acknowledgements. We acknowledge the help of Kameswara Rao during the data analysis. J.J.D.L., D.A.G.H., and A.M. acknowledge support provided by the Spanish Ministry of Economy and Competitiveness (MINECO) under grant AYA−2014−58082−P. D.A.G.H. was funded by the Ramón y Cajal fellowship number RYC−2013−14182. This work is based on observations obtained with ESO/VLT under the programme 290.D-5093(A).

References

Allamandola, L. J., Tielens, A. G. G. M., & Barker, J. R. 1985, ApJ, 290, L25
Bauschlicher, C. W., Boersma, C., Ricca, A., et al. 2010, ApJS, 189, 341
Beaulieu, S. F., Dopita, M. A., & Freeman, K. C. 1999, ApJ, 515, 610
Bernard-Salas, J., Cami, J., Peeters, E., et al. 2012, ApJ, 757, 41
Boersma, C., Bauschlicher, C. W., Ricca, A., et al. 2014, ApJS, 211, 8
Cami, J., Bernard-Salas, J., Peeters, E., & Malek, S. E. 2010, Science, 329, 1180
Cataldo, F., & Iglesias-Groth, S. 2009, MNRAS, 400, 291
Cataldo, F., García-Hernández, D. A., & Manchado, A. 2014, Eur. Chem. Bull., 3, 740
Cataldo, F., García-Hernández, D. A., & Manchado, A. 2015, FNCN, 23, 818
Chiar, J. E., Tielens, A. G. G. M., Whittet, D. C. B., et al. 2000, ApJ, 537, 749
Cox, N. L. J. 2011, in PAHs and the Universe: A Symposium to Celebrate the 25th Anniversary of the PAH Hypothesis, eds. C. Joblin, & A. G. G. M. Tielens, EAS Pub. Ser., 46
Cutri, R. M., et al. 2012, VizieR On-line Data Catalog: II/311
De Bruijne, J. H. J., & Eilers, A. -C. 2012, A&A, 546, A61
Díaz-Luis, J. J., García-Hernández, D. A., D. A., Rao, N. K., et al. 2015, A&A, 573, A97
Duley, W. W., & Williams, D. A. 1981, MNRAS, 196, 269
Duley, W. W., & Williams, D. A. 2011, ApJ, 737, L44
Duley, W. W., & Hu, A. 2012, ApJ, 745, L11
Gadallah, K. A. K., Mutschke, H., & Jager, C. 2013, A&A, 554, A12
García-Hernández, D. A., & Díaz-Luis, J. J. 2013, A&A, 550, L6
García-Hernández, D. A., Manchado, A., García-Lario, P., et al. 2010, ApJ, 724, L39
García-Hernández, D. A., Iglesias-Groth, S., Acosta-Pulido, J. A., et al. 2011a, ApJ, 737, L30
García-Hernández, D. A., Rao, N. K., & Lambert, D. L. 2011b, ApJ, 729, 126
García-Hernández, D. A., Villaver, E., García-Lario, P., et al. 2012, ApJ, 760, 107
García-Hernández, D. A., Cataldo, F., & Manchado, A. 2013, MNRAS, 434, 415
García-Lario, P., Manchado, A., Ulla, A., Manteiga, M. 1999, ApJ, 513, 941
Gudennavar, S. B., Bubbly, S. G., Preethi, K., et al. 2012, ApJ, 199, 8
Iglesias-Groth, S. 2007, ApJ, 661, L167
Iglesias-Groth, S., & Esposito, M. 2013, ApJ, 776, L2
Iglesias-Groth, S., Cataldo, F., & Manchado, A. 2011, MNRAS, 413, 213
Iglesias-Groth, S., García-Hernández, D. A., Cataldo, F., et al. 2012, MNRAS, 423, 2868
Jourdain de Muizon, M., D'Hendecourt, L. B., & Geballe, T. R. 1990, A&A, 227, 526
Kroto, H. W., Heath, J. R., Obrien, S. C., et al. 1985, Nature, 318, 162
Kwok, S., & Zhang, Y. 2011, Nature, 479, 80
Kwok, S., Volk, K., & Hrivnak, B. J. 1989, ApJ, 345, L51
Kwok, S., Volk, K., & Hrivnak, B. J. 1999, A&A, 350, L35
Leger, A., & Puget, J. L. 1984, A&A, 137, L5
Maltseva, E., Petrignani, A., Candian, A., et al. 2015, ApJ, 814, 23
Otsuka, M., Kemper, F., Cami, J., et al. 2014, MNRAS, 437, 2577
Russell, R. W., Soifer, B. T., & Merrill, K. M. 1977, ApJ, 213, 66
Sadjadi, S. A., Zhang, Y., & Kwok, S. 2015, ApJ, 807, 95
Scott, A., Duley, W. W., & Pinho, G. P. 1997, ApJ, 489, L193
Sellgren, K., Uchida, K. I., & Werner, M. W. 2007, ApJ, 659, 1338
Sellgren, K., Werner, M. W., Ingalls, J. G., et al. 2010, ApJ, 722, L54
Smith, E. C. D., & McLean, I. S. 2008, ApJ, 676, 408
Soubiran, C., Jasniewicz, G., Chemin, L., et al. 2013, A&A, 552, A64
Sturm, E., Lutz, D., Tran, D., et al. 2000, A&A, 358, 481
Tokunaga, A. T., Sellgren, K., Smith, R. G., et al. 1991, ApJ, 380, 452
Volk, K., Hrivnak, B. J., Matsuura, M., et al. 2011, ApJ, 735, 127
Wang, W., & Liu, X.-W. 2007, MNRAS, 381, 669
Webster, A. 1995, MNRAS, 277, 1555
Wegner, W. 2003, Astron. Nachr., 324, 219
Williams, R., Jenkins, E. B., Baldwin, J. A., et al. 2008, ApJ, 677, 1100
Zhang, Y., & Kwok, S. 2011, ApJ, 730, 126
Zhang, Y., & Kwok, S. 2013, Earth, Planets and Space, 65, 1069